

A Clarke-Wavelet-Based Time-Domain Power Transformer Differential Protection

Medeiros, R.P.; Costa, F.B.; Silva, K.M.; Chavez, J.J.; Popov, M.; Lima Junior, J.R.

DOI

[10.1109/TPWRD.2021.3059732](https://doi.org/10.1109/TPWRD.2021.3059732)

Publication date

2022

Document Version

Final published version

Published in

IEEE Transactions on Power Delivery

Citation (APA)

Medeiros, R. P., Costa, F. B., Silva, K. M., Chavez, J. J., Popov, M., & Lima Junior, J. R. (2022). A Clarke-Wavelet-Based Time-Domain Power Transformer Differential Protection. *IEEE Transactions on Power Delivery*, 37(1), 317-328. <https://doi.org/10.1109/TPWRD.2021.3059732>

Important note

To cite this publication, please use the final published version (if applicable). Please check the document version above.

Copyright

Other than for strictly personal use, it is not permitted to download, forward or distribute the text or part of it, without the consent of the author(s) and/or copyright holder(s), unless the work is under an open content license such as Creative Commons.

Takedown policy

Please contact us and provide details if you believe this document breaches copyrights. We will remove access to the work immediately and investigate your claim.






Green Open Access added to TU Delft Institutional Repository

'You share, we take care!' - Taverne project

<https://www.openaccess.nl/en/you-share-we-take-care>

Otherwise as indicated in the copyright section: the publisher is the copyright holder of this work and the author uses the Dutch legislation to make this work public.

A Clarke-Wavelet-Based Time-Domain Power Transformer Differential Protection

Rodrigo Prado Medeiros , Flavio Bezerra Costa , *Member, IEEE*, Kleber Melo Silva , *Senior Member, IEEE*, Jose de Jesus Chavez Muro , *Member, IEEE*, Jose Raimundo Lima Júnior, and Marjan Popov , *Senior Member, IEEE*

Abstract—Phasor-based differential protection is widely used as the main protection function of the power transformer due to its reliability and ability to discriminate internal from external faults and inrush currents. However, these methods present some delays due to phasor convergence during the fault occurrence and can fail during challenging situations, such as transformer energizations with low second-harmonic content and turn-to-turn and turn-to-ground internal faults. This paper proposes a novel time-domain power transformer differential protection based on Clarke and wavelet transforms with only one differential unit and with automatic setting to be used in any power transformer. Considering both actual and simulation data, the performance validation reveals that the proposed method is efficient, ultra-fast, simple, and independent of the fundamental and harmonic components of the differential current. The method was also implemented in a real-time digital simulator to demonstrate its practical feasibility.

Index Terms—ATP-EMTP, clarke transform, differential protection, power transformers, RTDS, wavelet transform.

I. INTRODUCTION

POWER transformers are widely used in power systems, and faults on these equipment must be isolated as fast as possible. Therefore, power transformer protection must detect internal faults with high sensitivity and speed, guaranteeing no operation for external faults and energization maneuvers [1].

The differential protection is the commonly applied protection for power transformers rated from 10 MVA [2], for which percentage differential relays or high impedance relays are mainly

used for this purpose [3]. Percentage differential relays operate when the differential current measured at the transformer terminals exceeds a predefined percentage of the restraint current. Although differential relays are commonly used, they must present a suitable adjustment to take into account the transformer tap changer, errors due to CT saturation, transformer overexcitation, and inrush currents.

Aiming to improve the conventional percentage differential relays, additional harmonic restraint and harmonic blocking methods have been used [4], [5]. Although those methods provide security, the internal fault detection can be delayed due to the digital filtering process to compute harmonic components. Furthermore, these methods may fail during inrush conditions because the second harmonic content may be smaller than established thresholds, causing relay misoperation [6]. Besides harmonic-based functions, a negative sequence unit is also commonly used for detecting unbalanced internal faults, such as turn-to-turn and turn-to-ground faults. However, this unit is usually blocked during external faults and transformer energizations [7].

Several techniques based on artificial intelligence, digital signal processing, and probability theory and statistics have been developed in order to improve the efficiency of transformer differential protection schemes [8]–[11]. For instance, in [8] a method based on the Clarke transform and fuzzy logic to single out internal faults on power transformers is presented. Clarke transform was applied on instantaneous values of differential currents, which eliminated the need of a phasor estimation algorithm and reduced the computational burden. However, the method did not ensure the protection for turn-to-ground faults between the first 5% and the neutral point of the wye-connected winding. Furthermore, the performance of the method was not assessed for CT saturation.

Research reported in [9] and [11] used high-order statistics and the second central moment techniques to distinguish between internal faults and energizations, respectively. Both methods presented good success rates in the event discrimination, but only [11] reported adjusts with no dependence of the transformer and system parameters. However, these methods did not consider transformer overexcitation, which is an important situation for validating new power transformer protections.

The wavelet transform has been widely employed to assist power transformer differential protection [10], [12]–[15]. In [13], using the real-time boundary stationary wavelet

Manuscript received August 5, 2020; revised November 15, 2020 and January 16, 2021; accepted February 9, 2021. Date of publication February 16, 2021; date of current version January 24, 2022. This work was supported by CAPES (Coordenação de Aperfeiçoamento de Pessoal de Nível Superior) and CNPq (Conselho Nacional de Desenvolvimento Científico e Tecnológico). Paper no. TPWRD-01207-2020. (*Corresponding author: Rodrigo Prado Medeiros.*)

Rodrigo Prado Medeiros is with the UFRSA, Caraúbas-RN 59780, Brazil (e-mail: digaum_34@hotmail.com).

Flavio Bezerra Costa is with the School of Science and Thecnology, Federal University of Rio Grande do Norte, Natal-RN 59078-970, Brazil (e-mail: flaviocosta@ect.ufrn.br).

Kleber Melo Silva is with the Department of Electrical Engineering, University of Brasília, Brasília-DF 70910-900, Brazil (e-mail: klebermelo@unb.br).

Jose de Jesus Chavez Muro and Marjan Popov are with the Electrical Sustainable Energy, TU Delft, 2628CD Delft, Netherlands (e-mail: J.J.ChavezMuro@tudelft.nl; M.Popov@tudelft.nl).

Jose Raimundo Lima Júnior is with the University of Pernambuco, 225112, Recife-PE 50100-010, Brazil (e-mail: raimundol@gmail.com).

Color versions of one or more figures in this article are available at <https://doi.org/10.1109/TPWRD.2021.3059732>.

Digital Object Identifier 10.1109/TPWRD.2021.3059732

transform (RT-BSWT), the conventional phase (87T) and negative sequence (87Q) differential functions were recreated in the wavelet domain, such that they were named as 87TW and 87QW units, respectively. Instead of the phasor-based conventional differential protection, this method uses only high-frequency components of CT secondary currents. Hence, neither fundamental nor low-order harmonic components are necessary. This method presented: simplicity of implementation, fast operation, good accuracy, and low computational burden. However, the method described in [13] is affected by CT saturation, evolving external-to-internal faults, and transformer energization with or followed by faults. Therefore, the method presented in [13] was updated in [14] and [15] with additional functions to overcome these issues. Considering these three references [13]–[15], the performance assessment included general and challenging cases for the transformer differential protection, such as external faults with and without CT saturation, evolving external-to-internal faults, transformer energization followed by internal faults, sympathetic energizations, and several types of internal faults considering few percentage of the winding. The 87TW and 87QW units proposed in [13]–[15], which are segregated by phase, provided a better performance and a faster fault detection than the respective conventional ones. However, the performance of these wavelet-based methods was assessed only in a simulation environment and, therefore, with no validation by using actual records. Furthermore, the negative sequence unit was blocked during external faults, and the performance of these methods was not assessed for transformer overexcitations.

This paper proposes a power transformer differential protection by using both Clarke and wavelet transforms, named as 87TW α , which extracts high-frequency transients induced by faults to provide a fast operation in accordance with the time-domain operation instead of the phasor-based idea. While [13]–[15] use positive and negative units segregated by phase and additional inrush and CT saturation detection methods, the proposed method presents only the 87TW α unit, with no phase segregation. In addition, all equations present only addition and multiplication operations, and were designed to run in a real-time processing. Although the proposed method presents only one differential unit, it presents an automatic parameter setting to be used in any power transformer interchangeably. Furthermore, the proposed 87TW α unit can be used in power transformers with any number of windings.

A differential protection based on high-frequency transients induced by faults, such as proposed in this paper, requires currents in both transformer terminals sampled at a high rate compared to sampling frequencies used by conventional protective relays. Therefore, actual data to validate these methods are not readily available. Nevertheless, the proposed method was validated with actual records from a power transformer in an actual transmission power system, containing internal fault, external fault, external fault clearance, and transformer energization, where the actual relay failed in the last one. Moreover, the proposed method was further assessed by using representative simulations of internal faults, external faults with and without CT saturation, evolving external-to-internal faults, transformer overexcitations, transformer energizations,

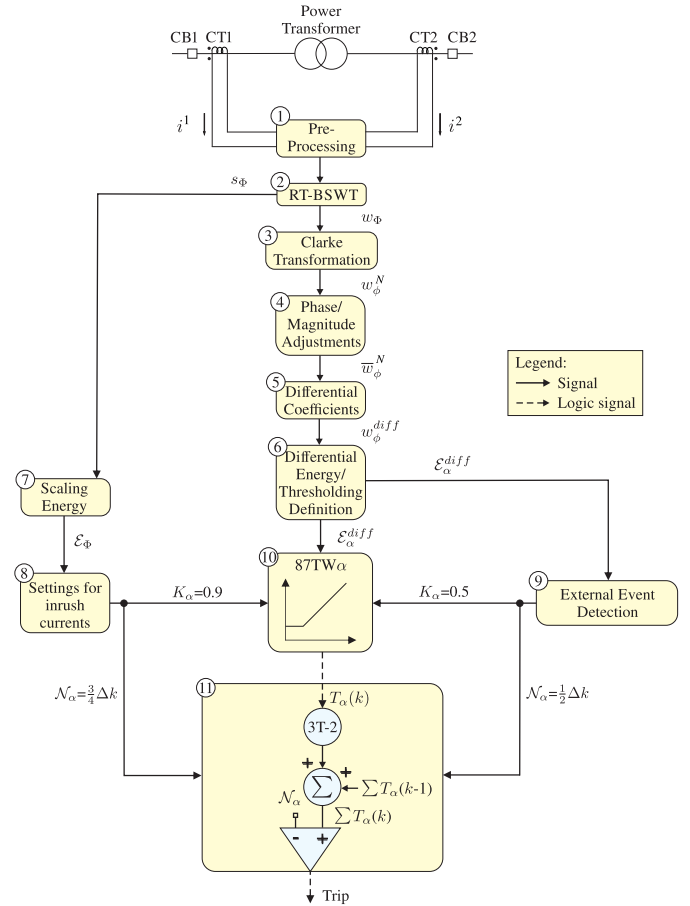


Fig. 1. The proposed Clarke-wavelet-based differential protection.

transformer energizations followed by internal faults, and sympathetic transformer energizations. The results revealed the proposed method was accurate, fast, and simple. The method was also implemented and evaluated in the Real Time Digital Simulator (RTDS) to demonstrate its practical applicability.

II. THE PROPOSED WAVELET-BASED TRANSFORMER DIFFERENTIAL PROTECTION

Fig. 1 depicts the block diagram of the proposed Clarke-wavelet-based power transformer differential protection, which is executed at each sampling time. The proposed method and its related equations were designed to run in a real-time application. Details about each block are addressed in the remainder of this section.

A. Basic Pre-Processing (Block 1)

The relay performs the digital acquisition of three-phase CT secondary currents by means of anti-aliasing filters and AD converters in order to get the following time-discrete currents: $i^N = \{i_A^N, i_B^N, i_C^N\}$. The sub-index $N = \{1, 2, 3, \dots, n\}$ refers to the n th transformer winding, whereas A , B , and C refer to phases A, B, and C, respectively. For the sake of illustration simplicity, the flowchart of the proposed method in Fig. 1 is for a particular

case of a transformer with two windings, where $N = 1$ for the primary winding and $N = 2$ for the secondary winding.

B. RT-BSWT (Block 2)

The scaling and wavelet coefficients of the RT-BSWT are respectively given by [16]:

$$s_{\Phi}(l, k) = \frac{1}{\sqrt{2}} \sum_{n=0}^{L-1} h_{\varphi}(n) \overset{\circ}{i}_{\Phi}(k - L + n + 1 + l), \quad (1)$$

$$w_{\Phi}(l, k) = \frac{1}{\sqrt{2}} \sum_{n=0}^{L-1} h_{\psi}(n) \overset{\circ}{i}_{\Phi}(k - L + n + 1 + l), \quad (2)$$

where $k \geq \Delta k - 1$ is always associated to the current sample time k/f_s , in which f_s is the sampling frequency; $0 \leq l < L$ is the border index; h_{φ} and h_{ψ} are low-pass scaling and high-pass wavelet filters, respectively; L is the filter length; $\Delta k \geq L$ is the sliding window length; $\overset{\circ}{i}_{\Phi}(k + m) = i_{\Phi}(k - \Delta k + m)$ with $m \in \mathbb{N}^*$, which is a periodized current in Δk samples; $s_{\Phi} = \{s_A^N, s_B^N, s_C^N\}$ and $w_{\Phi} = \{w_A^N, w_B^N, w_C^N\}$ are related to $i_{\Phi} = \{i_A^N, i_B^N, i_C^N\}$.

C. The Clarke Transform (Block 3)

This paper proposes the application of the Clarke transform in the instantaneous boundary wavelet coefficients in order to compute the alpha-mode (α -mode) wavelet coefficients (Clarke-wavelet coefficients), as follows:

$$\begin{bmatrix} w_{\alpha A}^N(k) \\ w_{\alpha B}^N(k) \\ w_{\alpha C}^N(k) \end{bmatrix} = \sqrt{\frac{2}{3}} \begin{bmatrix} 1 & -\frac{1}{2} & -\frac{1}{2} \\ -\frac{1}{2} & 1 & -\frac{1}{2} \\ -\frac{1}{2} & -\frac{1}{2} & 1 \end{bmatrix} \begin{bmatrix} w_A^N(k) \\ w_B^N(k) \\ w_C^N(k) \end{bmatrix}, \quad (3)$$

where $w_{\phi}^N = \{w_{\alpha A}^N, w_{\alpha B}^N, w_{\alpha C}^N\}$ are the respective α -mode wavelet coefficients related to the primary transformer winding currents $i_{ABC}^N = \{i_A^N, i_B^N, i_C^N\}$; $\phi = \{\alpha A, \alpha B, \alpha C\}$.

D. Phase/Magnitude Adjustments (Block 4)

The magnitude, phase shift, and zero-sequence correction are performed on the α -mode wavelet coefficients as follows:

$$\begin{bmatrix} \bar{w}_{\alpha A}^N \\ \bar{w}_{\alpha B}^N \\ \bar{w}_{\alpha C}^N \end{bmatrix} = \frac{1}{TAP_N} M_N \begin{bmatrix} w_{\alpha A}^N \\ w_{\alpha B}^N \\ w_{\alpha C}^N \end{bmatrix}, \quad (4)$$

where $\bar{w}_{\phi}^N = \{\bar{w}_{\alpha A}^N, \bar{w}_{\alpha B}^N, \bar{w}_{\alpha C}^N\}$; TAP_N is the tap of the CT; and M_N is the matrix used for the transformer angular displacement [17], [18].

E. Differential Wavelet Coefficients (Block 5)

Based on the classical differential currents [19], this paper proposes the differential Clarke-wavelet coefficients instead of

differential currents. The differential α -mode wavelet coefficients are given by:

$$w_{\phi}^{op}(0, k) = \sum_{m=1}^N \frac{1}{2} \bar{w}_{\phi}^m(0, k), \quad (5)$$

$$w_{\phi}^{op}(l \neq 0, k) = \sum_{m=1}^N \bar{w}_{\phi}^m(l, k), \quad (6)$$

where $0 \leq l < L$; $w_{\phi}^{op} = \{w_{\alpha A}^{op}, w_{\alpha B}^{op}, w_{\alpha C}^{op}\}$; m is the counter for the number of windings; and the superscript *op* refers to operation Clarke-wavelet coefficients.

F. Differential Energy and the Automatic Threshold Definition (Block 6)

Based on [16], this paper proposes the differential Clarke-mode wavelet coefficient energies, named as differential Clarke-mode energies ($\mathcal{E}_{\phi}^{diff} = \{\mathcal{E}_{\phi}^{op}, \mathcal{E}_{\phi}^{res}\}$), where:

$$\mathcal{E}_{\phi}^{op}(k) = \sum_{l=1}^{L-1} [w_{\phi}^{op}(l, k)]^2 + \sum_{n=k-\Delta k+L}^k [w_{\phi}^{op}(0, n)]^2, \quad (7)$$

and

$$\mathcal{E}_{\phi}^{res}(k) = \sum_{m=1}^N \mathcal{E}_{\phi}^m(k), \quad (8)$$

where $0 \leq l < L$; $\mathcal{E}_{\phi}^{op} = \{\mathcal{E}_{\alpha A}^{op}, \mathcal{E}_{\alpha B}^{op}, \mathcal{E}_{\alpha C}^{op}\}$; and $\mathcal{E}_{\phi}^m(k)$ is the wavelet coefficient energy of the current of the m th winding, being computed in the same way as \mathcal{E}_{ϕ}^{op} .

The α_A -, α_B -, and α_C -modes are combined into just one α -mode energy as follows:

$$\mathcal{E}_{\alpha}^{op}(k) = \mathcal{E}_{\alpha A}^{op}(k) + \mathcal{E}_{\alpha B}^{op}(k) + \mathcal{E}_{\alpha C}^{op}(k), \quad (9)$$

$$\mathcal{E}_{\alpha}^{res}(k) = \mathcal{E}_{\alpha A}^{res}(k) + \mathcal{E}_{\alpha B}^{res}(k) + \mathcal{E}_{\alpha C}^{res}(k). \quad (10)$$

Therefore, α -mode protection is not segregated by phase, and this block returns only two differential energy variables: $\mathcal{E}_{\alpha}^{diff} = \{\mathcal{E}_{\alpha}^{op}, \mathcal{E}_{\alpha}^{res}\}$.

The threshold related to the energy $\mathcal{E}_{\alpha}^{diff}$ is automatic defined as follows:

$$E_{\alpha}^{diff} = \frac{P}{k_2 - k_1 + 1} \sum_{n=k_1}^{k_2} \mathcal{E}_{\alpha}^{diff}(n), \quad (11)$$

where $[k_1/f_s, k_2/f_s]$ is a previous steady-state time range and $P = 5$. These thresholds are essential for detecting events after the steady-state, such as internal faults, external faults, and transformer energization maneuvers, and are automatically defined to a specific power transformer based on the noise statistic.

G. Scaling Coefficient Energy (Block 7)

Conversely to the wavelet coefficient energy, the scaling coefficient energy of the currents are directly proportional to low-frequency components, which is ideal to identify null-currents before transformer energization. Based on [16], the scaling

coefficient energies are given by:

$$\mathcal{E}_\Phi(k) = \sum_{l=1}^{L-1} [s_\Phi(l, k)]^2 + \sum_{n=k-\Delta k+L}^k [s_\Phi(0, n)]^2, \quad (12)$$

where $\mathcal{E}_\Phi = \{\mathcal{E}_{sA}^N, \mathcal{E}_{sB}^N, \text{ and } \mathcal{E}_{sC}^N\}$ is the scaling coefficient energy of $i_\Phi = \{i_A^N, i_B^N, \text{ and } i_C^N\}$.

H. Settings for Inrush Currents (Block 8)

The transformer can be identified as opened when currents are lower than pickup values, which is accomplished in the wavelet domain as follows:

$$\mathcal{E}_\Phi(k) < E_\Phi, \quad (13)$$

where E_Φ are thresholds related to \mathcal{E}_Φ .

When (13) is fulfilled, the method automatically sets the 87TW α unit slope to $K_\alpha = 0.9$, sets the trip delay to $\mathcal{N}_\alpha = \frac{3}{4}\Delta k$, and generates the pre-energization flag. The slope K_α and the trip delay \mathcal{N}_α are updated to make the protection more secure during transformer energizations without sacrificing its reliability in detecting internal faults during inrush currents. Then, the 87TW α unit will be able to recognize if the next event will be related to an inrush current with or without a permanent internal fault.

I. Inception Time Detection of External Events (Block 9)

According to the power transformer differential protection theory, the ratio I_{op}/I_{res} tends to remain lower than the slope in external events to the power transformer protection zone, such as external faults, transformer overexcitations and sympathetic inrush conditions, avoiding possible relay misoperations [20], where I_{res} and I_{op} are operating and restraining currents at the fundamental frequency (low-frequency components). Based on this premise, but using high-frequency components extracted with Clarke-wavelet differential energy, external events are detected if:

$$\mathcal{E}_\alpha^{op}(k) < K_\alpha \mathcal{E}_\alpha^{res}(k) \quad (14)$$

and

$$\begin{cases} \mathcal{E}_\alpha^{op}(k-1) < E_\alpha^{op} \\ \mathcal{E}_\alpha^{res}(k-1) < E_\alpha^{res} \\ \mathcal{E}_\alpha^{res}(k) > E_\alpha^{res} \end{cases} \quad (15)$$

where $k_{EF}/f_s = k/f_s$ is the detected external fault inception time when both (14) and (15) are fulfilled.

When both (14) and (15) are met, the method sets $K_\alpha = 0.5$ and $\mathcal{N}_\alpha = \frac{1}{2}\Delta k$, automatically. Then, the 87TW α unit will be able to properly detect possible internal faults after external ones (evolving external-to-internal fault), as well as CT and power transformer saturations in external events.

J. Differential Protection Units (Block 10)

Based on the classical differential principle, the proposed 87TW α unit detects an internal fault when:

$$\begin{cases} \mathcal{E}_\alpha^{op}(k) > K_\alpha \mathcal{E}_\alpha^{res}(k) \\ \mathcal{E}_\alpha^{op}(k) > E_\alpha^{op} \end{cases}. \quad (16)$$

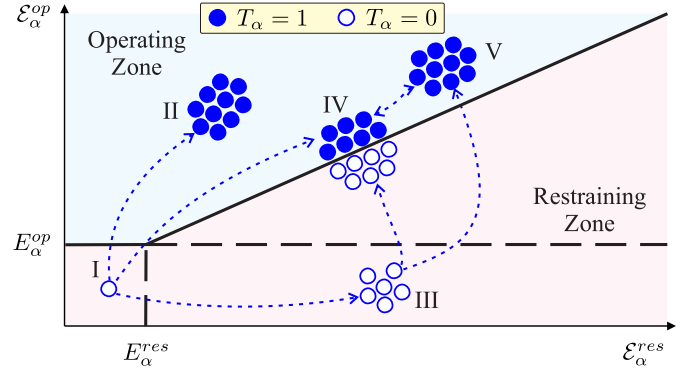


Fig. 2. Trajectory of the energy operating points for the most of events.

The default slope is $K_\alpha = 0.5$. However, it can change according to Sections II-H and II-I.

When a pre-energization flag is generated and (16) is fulfilled, the algorithm identifies the beginning of a transformer energization and the threshold E_α^{op} is then updated along the time in order to provide security during the occurrence of this event, as follows:

$$E_\alpha^{op} = M \mathcal{E}_\alpha^{op}(k), \quad \text{if } \mathcal{E}_\alpha^{op}(k) > \mathcal{E}_\alpha^{op}(k-1), \quad (17)$$

where $M = 0.01$ and $E_\alpha^{op} = 0$ at the beginning of the energization.

The inception time of the internal fault (k_{IF}/f_s) is identified when (16) is true and when

$$\begin{cases} \mathcal{E}_\alpha^{op}(k-1) < E_\alpha^{op} \\ \mathcal{E}_\alpha^{res}(k-1) < E_\alpha^{res} \end{cases} \quad (18)$$

is also true, where $k_{IF}/f_s = k/f_s$.

When (16) is true, the α -mode energy $\mathcal{E}_\alpha^{diff}$ is in the operation region and the trip command of the 87TW α unit is high ($T_\alpha(k) = 1$), otherwise $\mathcal{E}_\alpha^{diff}$ is in the restraining region and $T_\alpha(k) = 0$.

K. Trip Management (Block 11)

When the α -mode energy point is in the restraining region, then $T_\alpha(k) = 0$. Therefore, the operator $3T_\alpha - 2 = -2$, which produces a decrease by 2 in the trip counter $\Sigma T_\alpha(k)$, where $\Sigma T_\alpha(k) \geq 0$. Conversely, when the α -mode energy point is in the operating region, then $T_\alpha(k) = 1$. As a consequence, $3T_\alpha - 2 = 1$, which produces an increase in the trip counter $\Sigma T_\alpha(k)$. Thereafter, $\Sigma T_\alpha(k)$ is compared to the related trip delay \mathcal{N}_α , where the relay trips when $\Sigma T_\alpha(k) > \mathcal{N}_\alpha$ (Fig. 1).

The default trip delay \mathcal{N}_α is zero. However, it can change according to Sections II-H and II-I.

L. Qualitative Analysis

Fig. 2 depicts the expected trajectory of operating points $\mathcal{E}_\alpha^{diff}$ along the differential plane during the most important events. The trip depends on the position of the differential energy $\mathcal{E}_\alpha^{diff}$ and the trip delay, which changes in accordance with the events as follows:

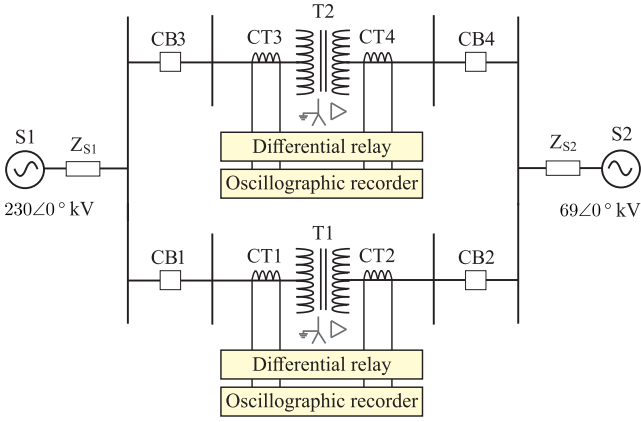


Fig. 3. Single line diagram of the electrical system.

- Steady-state period: $\mathcal{E}_\alpha^{diff}$ refers to the event I;
- Internal fault: $\mathcal{E}_\alpha^{diff}$ changes from I to II;
- External fault: $\mathcal{E}_\alpha^{diff}$ changes from I to III;
- External fault followed by CT saturation: $\mathcal{E}_\alpha^{diff}$ changes from I to III, and then from III to IV, where it stays more time in the restraining region;
- External fault followed by an internal fault: $\mathcal{E}_\alpha^{diff}$ changes from I to III, and then from III to V;
- Overexcitation: $\mathcal{E}_\alpha^{diff}$ changes from I to III, and then from III to IV, where it stays more time in the restraining region;
- Inrush current: $\mathcal{E}_\alpha^{diff}$ changes from I to IV, where it stays more time in the restraining region;
- Inrush current with permanent fault: $\mathcal{E}_\alpha^{diff}$ changes from I to II;
- Inrush current followed by a permanent fault: $\mathcal{E}_\alpha^{diff}$ changes from I to IV; When the internal fault starts, it changes from IV to V;

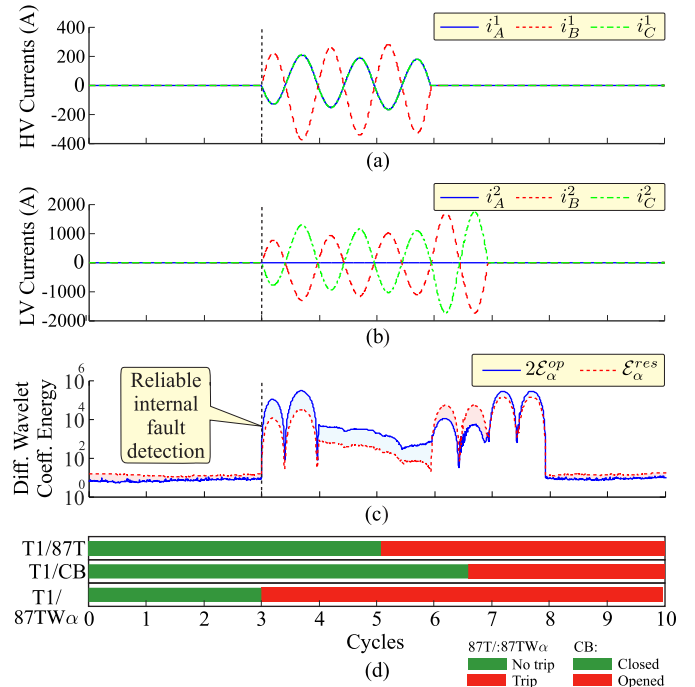
III. PERFORMANCE ASSESSMENT WITH ACTUAL DATA

This section presents a thorough discussion about the performance of an existing protection system used in an actual power transformer of a transmission system under internal fault, external fault, external fault clearance, and transformer energization as well as the performance of the proposed method.

A. Power System Description

Fig. 3 depicts the simplified single-line diagram of two actual power transformers of a power system where disturbances were recorded. The power system is represented by two equivalent sources (S1 and S2) for the sake of simplicity. T1 and T2 are 100 MVA, 230/69 kV power transformers configured at YNd1. The 230 kV and 69 kV CTs are connected at 500/5 A and 1200/5 A taps, respectively. Details about the system parameters are described in [15].

The traditional phasor-based 87 T function was used to protect the power transformer in the field. Nevertheless, a digital fault recorder (DFR) monitored the power transformers with a sampling frequency of 15360 Hz (256 samples per cycle of 60 Hz), where both currents and voltages at the high-voltage


 Fig. 4. Currents measurement in the transformer T1: (a) i_A^H , i_B^H , and i_C^H ; (b) i_A^X , i_B^X , and i_C^X ; (c) α -mode operating and restraining energies; (d) logic states for both circuit breakers and the differential relay which protects T1.

side (230 kV) as well as currents at the low-voltage side (69 kV) were measured as data records.

The proposed wavelet-based differential protection was assessed in an off-line analysis with the oscillographic records provided by the DFR at 15360 Hz. The proposed method runs with the Daubechies mother wavelet with four coefficients (db(4)).

B. Internal Fault

A double-line fault between phases B and C took place at the terminals of the monitored transformer T1. Therefore, it is an internal fault to the differential protection in T1. Fig. 4 depicts the currents measured in T1, the differential α -mode differential energies, and the digital status of the circuit breakers (T1/CB) and the differential protections (T1/87 T and T1/87TW α). The transformer differential relay operated correctly, providing the trip command to disarm T1 in about 2 cycles after the fault inception time. The high- and low-voltage circuit breakers opened in about four cycles after the fault inception time [Fig. 4(d)].

Fig. 5 depicts the trajectory of the differential α -mode energy operating points during the first cycle after the fault inception time. In this type of fault, the proposed 87TW α differential unit must trip when the operation energy points are two times higher than the restraining energy points after the internal fault inception time. Indeed, $\mathcal{E}_\alpha^{diff}$ presented a hard increase soon after the fault inception time ($2\mathcal{E}_\alpha^{op} \gg \mathcal{E}_\alpha^{res}$) and detected the internal fault successfully at 65 μ s (Figs. 4(c) and 5). Therefore, the trip provided by the proposed method would be faster than the actual relay with the conventional protection system such as shown in Fig. 4(d).

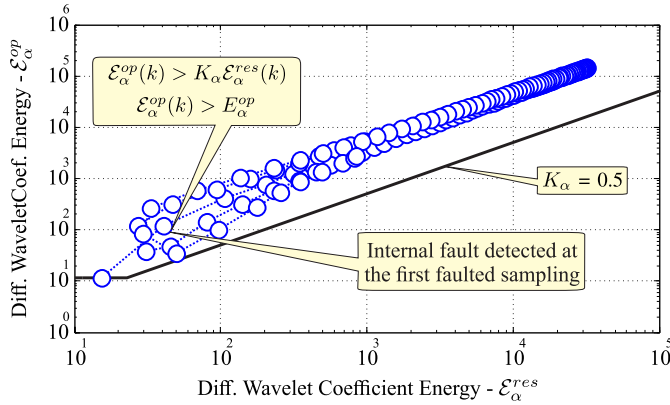


Fig. 5. α -mode energy operating points collected during the first cycle after internal fault initiation.

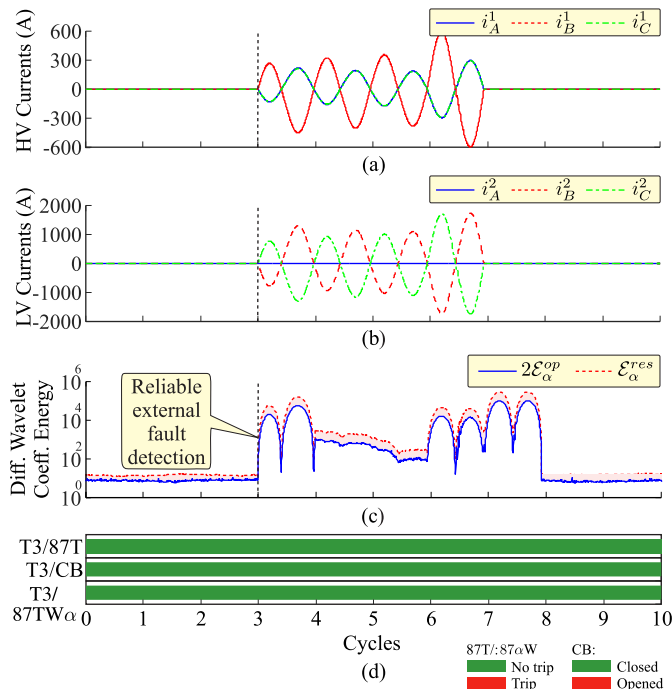


Fig. 6. Current measurement in transformer T2: (a) i_A^H , i_B^H , and i_C^H ; (b) i_A^X , i_B^X , and i_C^X ; (c) α -mode operating and restraining energies; (d) Logic states for both circuit breakers and differential relay that protect T2.

C. External Fault and External Fault Clearance

The AB fault inside the T1 protection zone, described as an internal fault to T1 in Section III-B, is an external fault to the differential relay that protects T2, as depicted in Fig. 3. Fig. 6 depicts the currents measured in the transformer T2, the differential α -mode energies, and the digital status of the circuit breakers and the differential protections due to the AB fault on T1. As expected, the differential relay of T2 did not trip. Therefore, the high- and low-voltage circuit breakers of T2 remained closed during the AB fault in T1 [Fig. 6(d)]. In addition, no false trip was issued by the relay in T2 during the external fault clearance. Therefore, the existing protection

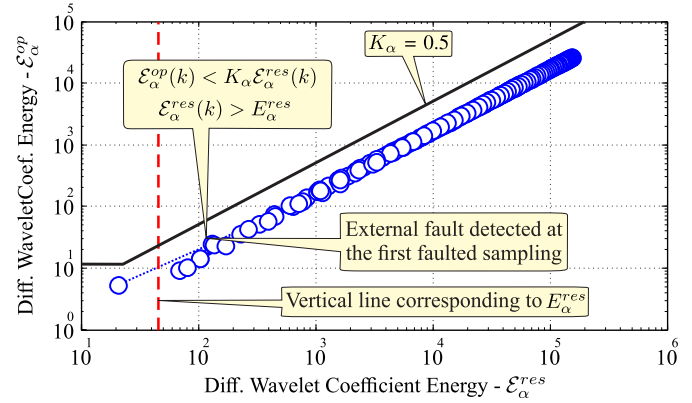


Fig. 7. α -mode energy operating points collected during the first cycle after external fault initiation.

system in T2 performed well for both the external fault and its clearance.

Fig. 7 depicts the trajectory of the differential α -mode energy operating points during the first cycle after the fault inception time. As expected, the 87TW α differential unit did not trip because $2E_{\alpha}^{op} \ll E_{\alpha}^{res}$ from the beginning of the external fault to its clearance.

D. Transformer Energization

The accurate detection of inrush currents is not a trivial task, even for existing commercial numerical differential relays. For instance, several commercial numerical relays need additional protection units based on the harmonic content, such as harmonic restraint and harmonic blocking logics. Nevertheless, there is no guarantee of a proper performance during inrush current, especially when the level of the second harmonic drops below a specific threshold [6].

An actual energization maneuver took place at the monitored transformer T1, in which the 230 kV terminal was energized under no load. Fig. 8 depicts the currents measured at the high-voltage side of the transformer T1, the scaling coefficient energy of the high-voltage CT currents, the α -mode differential energies, and the digital status of the circuit breaker CB1 and the actual differential protection. During the energization, the 2nd harmonic level of the phase C differential current dropped below the 15% limit adjustment established for the harmonic blocking function. Therefore, the transformer differential relay operated inadvertently, providing a wrong trip command to disarm T1, which was opened in about two cycles after the beginning of the maneuver. Therefore, Fig. 9 shows a case where the existing protection in an actual power system failed during a transformer energization. It is not the scope of this paper to address the performance of the existing protection system and its settings. Therefore, more details about this case are unknown.

In Fig. 8(b), before the energization, the scaling coefficient energy is below the threshold related to the transformer load current. Therefore, a pre-energization was detected by the proposed method in accordance with (13). Furthermore, the threshold E_{α}^{op} was updated according to (17) and the slope K_{α} was increased

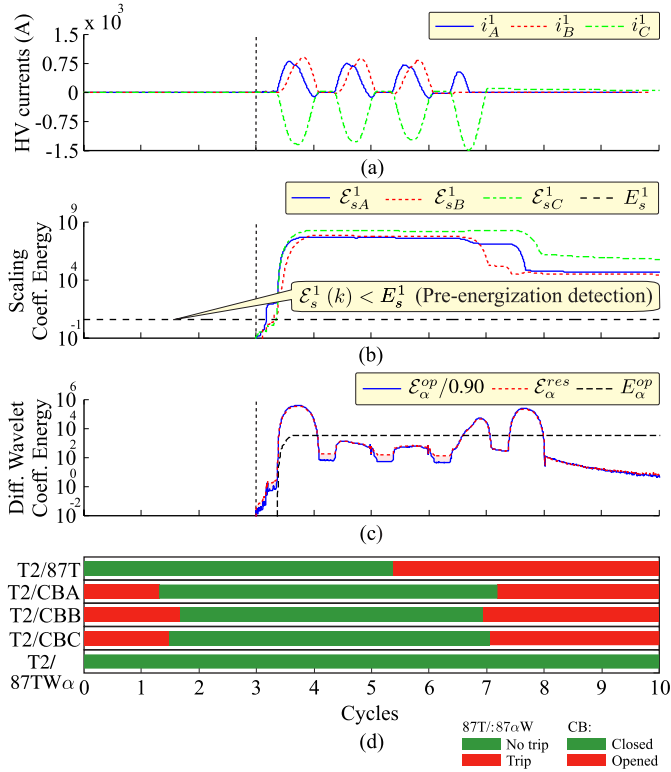


Fig. 8. (a) T1 HV CT Currents; (b) Scaling coefficient energy of the CT currents; (c) α -mode operating and restraining energies; (d) logic states for both circuit breakers and differential relay that protect T1.

to 0.9 from the beginning of the transformer energization in order to ensure security during the occurrence of this event. Nevertheless, the operating points moved to the operating region ($\mathcal{E}_\alpha^{op}/0.9 > \mathcal{E}_\alpha^{res}$), which could cause a relay misoperation. However, the operating points remained in the operation region for a short time due to the typical saturation during the inrush current [Fig. 9(c)]. This fact did not happen during the internal fault, in which $2\mathcal{E}_\alpha^{op} \gg \mathcal{E}_\alpha^{res}$ from the fault inception time to its clearance [Fig. 4(c)]. Therefore, this issue was properly solved with the updating of both E_α^{op} and K_α , as well as with the trip delay in association with the trip counter, where the trip remained blocked from the beginning of the transformer energization maneuver. Therefore, the transformer energization was properly detected by the wavelet-based differential protection and no wrong trip would be provided to disarm T1 if the proposed method was installed to protect this power transformer.

IV. PERFORMANCE ASSESSMENT WITH SIMULATION DATA

A power system with similar parameters to the actual system described in section III (Fig. 3) was simulated in the ATP/EMTP software environment for the performance assessment of the proposed method. Several challenging scenarios for the transformer differential protection were generated, as follows:

- 1) Database 1 (internal faults):
 - a) turn-to-turn faults on phase A wye winding; turn-to-turn faults on the delta winding between phases A and B; turn-to-ground faults on phase A wye winding; and

turn-to-ground faults on the delta winding between the A-to-B-winding and the earth. The percentage of the turns in the fault is equal to $e = \{1, 2, 3, \dots, 98\}\%$ (392 records).

- b) AG, BG, and CG faults on the high- and low-voltage terminals of T1, inside the protection zone, with the fault inception angle of $\theta_f = \{0, 30, 60, 90, 120, 150, 180\}$ electrical degrees and fault resistance of $R_f = \{100, 200, 300\} \Omega$ (126 records). θ_f corresponds to the phase A voltage angle at the fault point.
- 2) Database 2 (external faults + CT saturation): AG, BG, CG, AB, BC, AC, ABG, BCG, ACG, and ABC faults on the high- and low-voltage terminals of T1, but external to the T1 transformer protection zone, with $\theta_f = \{0, 30, 60, 90, 120, 150, 180\}$ electrical degrees and $R_f = \{1, 10\} \Omega$ (280 records). The burden of CTs was intentionally increased in order to impose CT saturation.
- 3) Database 3 (evolving external-to-internal faults): AG external faults with $\theta_f = 90^\circ$ and $R_f = 1 \Omega$ on the high and low voltage terminals of T1 evolving to turn-to-turn and turn-to-ground internal faults on transformer windings at the same side of the faulted terminal. The percentage of the turns in the internal fault is equal to $e = \{1, 2, 3, \dots, 98\}\%$ (392 records). Internal faults take place three cycles after the external faults.
- 4) Database 4 (transformer overexcitations): This event was induced by applying a 140% overvoltage on the T1 high voltage side with variations of $\theta_s = \{0, 1, 2, \dots, 179, 180\}$ electrical degrees (181 records), where θ_s is the phase A voltage angle at the overvoltage point.
- 5) Database 5 (transformer energizations): Switching performed by the high voltage side (230 kV) of T1, with its secondary terminal opened (CB2 opened) and with T2 de-energized (CB3 and CB4 opened), and changing the high voltage circuit breaker closing time at angles $\theta_s = \{0, 1, 2, \dots, 179, 180\}$ electrical degrees (181 records).
- 6) Database 6 (transformer energizations with permanent internal fault): Switching performed by the high voltage side of T1, with the secondary terminal opened (CB2 opened) as well as the transformer T2 opened, changing the high voltage circuit breaker closing time at angles $\theta_s = \{0, 90\}$ electrical degrees for each case listed on database 1 (784 records). There is a permanent internal fault at the switching time;
- 7) Database 7 (sympathetic inrushes): Switching performed by the high voltage side of T2, with its secondary terminal opened (CB4 opened) and with T1 previously energized (CB1 and CB2 closed), and changing: the high voltage circuit breaker closing time at angles $\theta_s = \{0, 30, 60, 90, 120, 150, 180\}$ electrical degrees, the load power factor $PF = \{0.7, 0.8, 0.9, 1.0\}$, and the X/R ratio of the circuit connected to the transformer high-voltage winding $X/R = \{10.0, 20.0\}$ (56 records).

The databases 1-7 were generated by considering a typical signal-to-noise relation (SNR) of 60 dB. The performance of the proposed method was compared to the traditional

TABLE I
THE CONVENTIONAL PROTECTION SCHEME PARAMETERIZATION [21], [22]

87T						87Q	
Harmonic restraint			Harmonic blocking				
$SLP1$	I_{puT}	K_2	K_5	K_{2b}	K_{5b}	$SLP2$	I_{puQ}
0.35	0.5 pu	0.15	0.15	0.15	0.15	0.25	0.1 pu

phasor-based differential functions: 87T with harmonic restraint and harmonic blocking units, and 87Q current differential elements, totaling two functions, where all of them are segregated by phase. The sampling frequency was $f_s = 1200$ Hz and the full-cycle Fourier algorithm was used in accordance with the real situation in section III. Table I describes the settings used for the conventional differential protection scheme according to relay manufacturers' recommendations [21], [22]. The 87Q unit is implemented with an intentional delay of two cycles in order to increase the security in its operation [18].

The proposed method presents only one function with neither phase segregation nor additional strategies such as harmonic restraint and harmonic blocking, and it runs at $f_s = 15360$ Hz, which is in accordance with the sampling frequency of the real data shown in Section III. Its setting are automatically defined one shown in Sections II and III.

Table II shows a performance comparison between both proposed and conventional methods regarding the success rate and the delay in detecting the events of the databases 1-7.

According to Table II, the external event detection module of the proposed method (block 9) presented robust performance for all cases of external faults with CT saturation, transformer overexcitations, and sympathetic inrushes, providing no trip (100% of success rate), and the inrush detection module (block 8) properly detected all single transformer energizations, presenting also a success rate of 100%, i.e., no trip in these cases. The conventional method also presented a success rate of 100%.

An example of the proposed method performance for external events is shown in Fig. 9, which depicts the CT currents and the alpha-mode differential energies in a 140% overvoltage on the 230 kV bus, but outside the transformer protection zone. According to Fig. 9(d), this event would be properly detected by the block 9 as an external event and no trip would be provided because $\Sigma T_\alpha(k) \ll \mathcal{N}_\alpha = \frac{1}{2}\Delta k$ during the event.

Regarding the internal faults (databases 1 and 2), the proposed 87TW α unit (block 10) was more accurate and faster than the conventional one, ensuring a success rate of 100% and detecting several faults with almost no change in the differential currents in which the conventional one failed, such as: turn-to-turn faults on the delta side with less of 5% of the shorted winding, and all the single-phase-to-ground faults between T1 and CT2 with $R_f = 300\Omega$.

The proposed 87TW α unit was also more reliable and faster than the conventional one regarding simultaneous events, such as evolving external-to-internal faults and transformer energizations with permanent internal faults, presenting success rates and average operating time, respectively, of 98.47% and 9.51 ms against 96.43% and 54.54 ms, for evolving external-to-internal

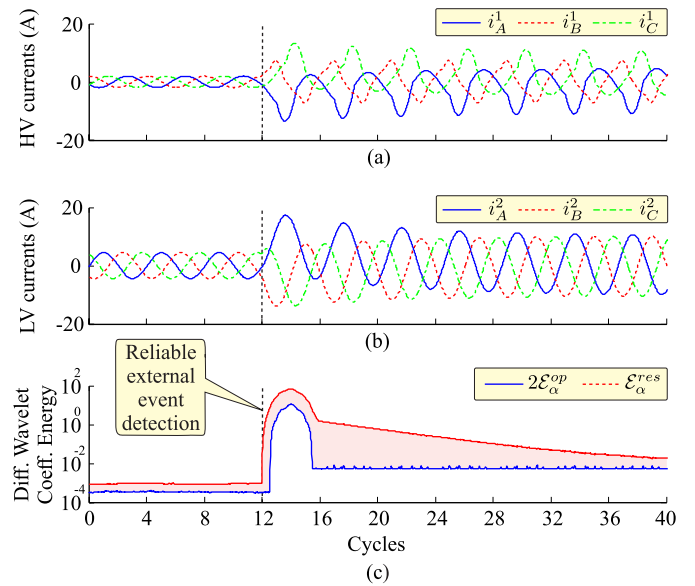


Fig. 9. Transformer overexcitation: (a) i_A^H , i_B^H , and i_C^H ; (b) i_A^X , i_B^X , and i_C^X ; (c) α -mode differential energies.

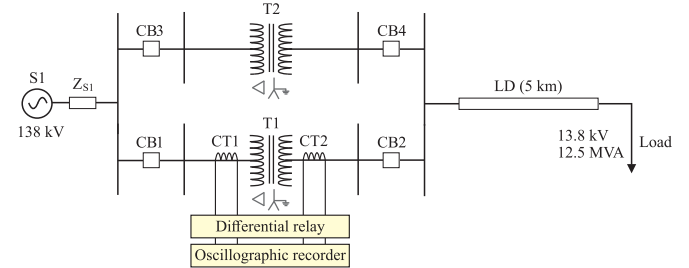


Fig. 10. Single-line diagram of the electrical system with two Dyn1 transformers in parallel.

faults, and 100% and 12.61 ms against 86.46% and 18.80 ms, for faulted transformer energizations.

V. PERFORMANCE ASSESSMENT IN ANOTHER POWER TRANSFORMER

The performance of the proposed method was also evaluated in another power transformer, with delta-star grounded configuration (Dyn1). Fig. 10 depicts the single-line diagram of the analyzed three-phase power system. The system consists of a 138 kV Thevenin equivalent connected to the primary winding of a transformer whose rated power is equal to 25MVA and ratio of 138:13.8 kV. A small distribution line connects a load of 10 MVA and power factor of 0.92 to the secondary winding of the transformer. The CTs connected to the primary and secondary windings of the power transformer presented transformation ratios equal to 200-5 and 2000-5 A, respectively. More details and information about the power system and power transformer parameters are find in [23].

The same cases of the databases 1, 2, 5, and 7 were generated in order to verify the performance of the proposed method. The proposed method was stable during external faults, transformer

TABLE II
PERFORMANCE ASSESSMENT OF THE METHOD FOR THE SIMULATED DATABASES

Event	Total cases	Proposed method			Conventional method		
		Correct operations	Success rate (%)	Average oper. time	Correct operations	Success rate (%)	Average oper. time
Internal faults (1.a)	392	392	100%	138 μ s	388	98.98%	15.84 ms
Internal faults (1.b)	126	126	100%	74 μ s	105	84%	29.06 ms
External faults	280	280	100%	-	280	100%	-
Evolving external-to-internal faults	392	386	98.47%	9.51 ms	378	96.43%	54.54 ms
Overexcitations	181	181	100%	-	181	100%	-
Energizations	181	181	100%	-	181	100%	-
Faulted energizations	784	784	100%	12.61 ms	677	86.46%	18.80 ms
Sympathetic inrush	56	56	100%	-	56	100%	-

energizations, and sympathetic energizations, i.e., none of these events were misdetected, as well as detected all internal faults (success rate of 100%) with an expressive average operating time of about 84 μ s. Therefore, these results are similar to the results obtained with the 100 MVA 230:69 kV power transformer in Section IV and suggest the good applicability of the proposed method for different power transformer configurations (power transformers with different vector groups).

VI. CASE STUDIES

A. A Single-Phase-to-Ground Fault Close to the Converter Transformer in an HVDC System

Faults close to transformers in line-commutated converters (LCC)-HVDC systems can lead to transformer differential protection relay misoperation due to high harmonic distortions in the AC currents of the transformers. The performance of the proposed method was assessed considering two fault scenarios in the LCC-HVDC of the CIGRE benchmark test system [24]: a single-phase-to-ground fault between the 12-pulse rectifier and the transformer, but external to the transformer protection zone (external fault); and a single-phase-to-ground fault within the transformer protection zone (internal fault). Both faults were simulated with a fault resistance of 10 Ω . More details of the LCC-HVDC system can be found in [24].

Fig. 11 depicts the CT currents and the alpha-mode differential energies monitored during the external fault. According to Figs. 13(a) and (b), the monitored currents on the AC side and on the converter side presented a high harmonic content. However, the proposed method was not affected and the external event was properly detected by the external fault detection module, and no trip was issued [Fig. 13(c)].

Fig. 12 depicts the CT currents and the alpha-mode differential energies monitored during the internal fault. Similarly to the external fault, the monitored currents on the AC side and on the converter side presented high harmonic content during the internal fault [Figs. 12(a) and (b)]. Despite the high distortion level in currents, the proposed $87TW_{\alpha}$ element properly detected the internal fault in the first cycle, 1.6 ms from the fault inception time.

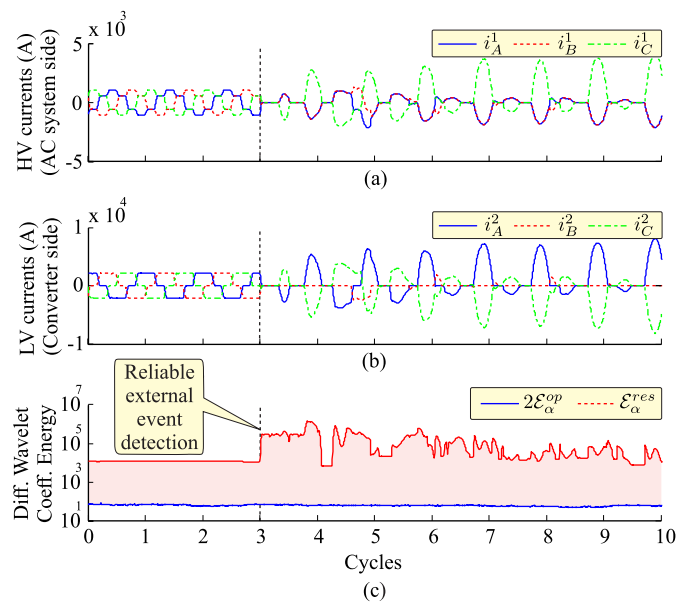


Fig. 11. A valve side single-phase-to-ground fault (external fault): (a) i_A^H , i_B^H , and i_C^H ; (b) i_A^X , i_B^X , and i_C^X ; (c) α -mode differential energies.

The proposed method was designed for detecting the highest frequency components in a current with sampling frequency of 15 360 Hz, i.e., the proposed method is sensitive for frequency components from 3840 to 7680 Hz. Therefore, it is expected a good performance even in the presence of DC component and low-frequency harmonics, such as shown in these two case studies. Nevertheless, it is necessary a more detailed evaluation of the proposed method in power transformers in HVDC systems in future works.

B. A Lightning Conduction by a Surge Arrester Installed on the Transformer Protection Zone

The impact on the proposed method performance caused by the operation of surge arresters within the transformer differential protection zone is discussed in this Section. For this analysis, the power system model shown in Fig. 3 was improved. A substation was modeled with the double bus single breaker

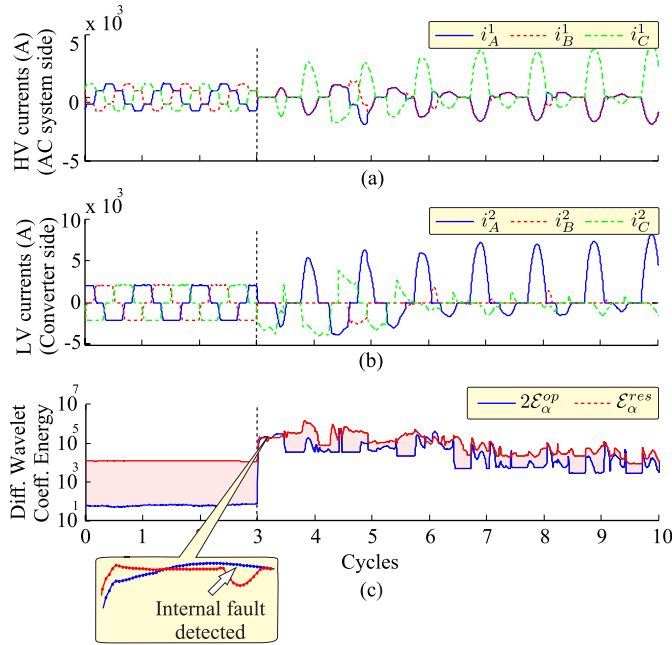


Fig. 12. A valve side single-phase-to-ground fault (internal fault): (a) i_A^H , i_B^H , and i_C^H ; (b) i_A^X , i_B^X , and i_C^X ; (c) α -mode differential energies.

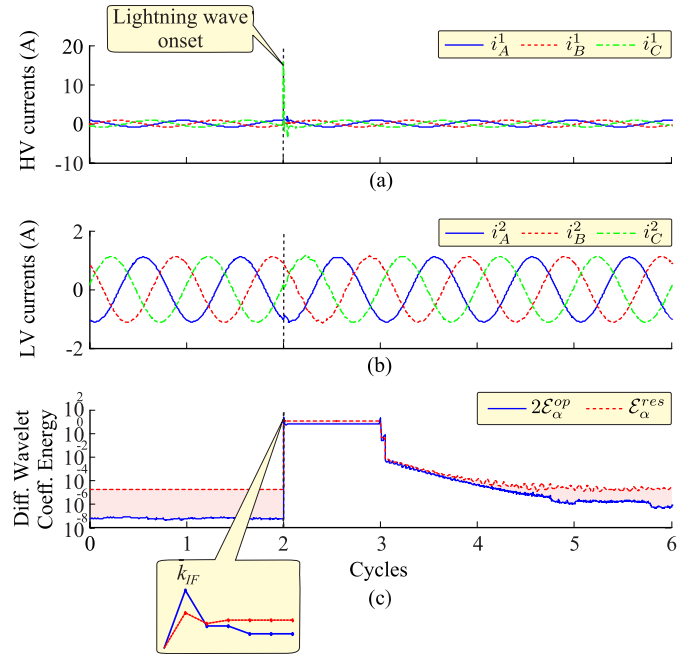


Fig. 13. A surge arrester conduction inside the transformer protection zone: (a) i_A^H , i_B^H , and i_C^H ; (b) i_A^X , i_B^X , and i_C^X ; (c) α -mode differential energies.

configuration [25], and the power transformers T1 and T2 as described in Section IV were connected to this substation. Moreover, a 230 kV transmission line 100 km long was modeled using the JMarti model [26]. Coupling capacitor voltage transformers (CCVTs) [27] and metal oxide varistor (MOVs) surge arresters [26] were considered in each bay. Typical stray capacitance values of power equipment such as circuit breakers, disconnect switches, power transformers, and busbar [27] were taken into account. A severe scenario was simulated considering a 10 kA lightning striking directly on the transmission line, 1 km away from the substation. The currents in the secondary of the CTs in the HV and LV sides of the protected transformer, as well as the alpha-mode differential energies, are shown in Fig. 13.

According to Fig. 13, the HV-side currents were affected by the lightning because the HV-side surge arresters are placed between the CT and the HV transformer winding. Conversely, the LV-side currents were weakly affected by the lightning because the HV-side surge arresters conducted during the lightning. Both operating and restraining energies increased soon after the surge transients in the power transformer. However, due to the fast and sharp decay of the surge wave, $2\mathcal{E}_\alpha^{op} > \mathcal{E}_\alpha^{res}$ just for one sampling time [Fig. 13(c)]. Therefore, a small time delay strategy could be used in the proposed protection to avoid the misdetection of internal faults when the surge arresters conduct during a lightning event. A more detailed evaluation of these cases will be accomplished in future works.

VII. COMPUTATIONAL BURDEN

The computational burden required by a protection method is an important parameter to verify the hardware implementation possibility. The basic requirement to a method run in real-time

is that the computational burden must be less than the sampling time $1/f_s$. Despite an offline assessment with massive data simulated in the ATP/EMTP program, the proposed method was implemented in the RTDS to demonstrate its practical feasibility, presenting computational burden less than 50 μ s. Another possibility to evaluate the computational burden is to compute the number of floating-point operations (FLOPs) required by a protection method. FLOPs are considered to be addition and multiplication operations. Memory management was not considered.

The proposed method needs only addition and multiplication operations, being quite simple. In addition, the number of FLOPs in the proposed method is regardless the sampling frequency. By using the mother wavelet db(4), a boundary wavelet coefficient energy only requires 34 FLOPs per sampling time, which is the same amount described in [16]. For any sampling frequency, the proposed algorithm needs 790 FLOPs per sampling time by using the mother wavelet db(4).

As a benchmark, the db(4) boundary wavelet coefficient energy was implemented in a floating-point DSP for a real-time analysis in [16], and the computational burden, per sampling time, related to 34 FLOPs was about 1.70 μ s. Considering the same proportion, the proposed method would require about 39.5 μ s per sampling time (7.2 μ s and 32.3 μ s would be the times required to perform the processing of the Clarke and wavelet transforms, respectively). Since the used sampling time is $1/f_s = 65 \mu$ s, the proposed method could be properly implemented in that specific DSP.

Considering all sines and cosines stored in a buffer instead of computing them during the execution time, such as shown in [28], the conventional method based on the Fourier algorithm requires addition, multiplication, and square root operations.

Square root operations consume several FLOPs depending on the DSP. In addition, the computational burden of the conventional Fourier-based method increases with the sampling frequency. For instance, considering a sampling frequency of $f_s = 1200$ Hz, such as set in this paper, the conventional method needs 2406 FLOPs + 21 square root operations per sampling time. This computational burden is higher than that provided by the proposed method. However, it must be accomplished during $1/f_s = 833.33\mu\text{s}$. By using the sampling frequency of the proposed method, i.e., $f_s = 15\,360$ Hz, the conventional method needs 27 894 FLOPs + 21 square root operations per sampling time. This strong number of FLOPs must be accomplished during $1/f_s = 65\mu\text{s}$, requiring a powerful DSP. Nevertheless, it is not necessary to evaluate the phasor-based protection at $f_s = 15\,360$ Hz, since one is interested until, at most, the 5th harmonic.

VIII. CONCLUSION

This paper proposed a new time-domain transformer differential protection based on the wavelet and Clarke transforms with only one differential unit (87TW α unit), which is without phase segregation and presents no need of additional harmonic content-based functions. The performance of the proposed method was compared to the conventional differential protection one considering both actual and simulated data.

Regarding the actual data, the existing conventional protection failed during an actual transformer energization due to the low harmonic content of the differential current, providing a wrong trip, whereas the proposed method was successful in an offline analysis of this case. Both existing and proposed methods properly detected the actual internal fault. However, the proposed method detected it in $65\mu\text{s}$ because it is based only in the high-frequency content of currents, whereas the existing one took about two cycles to provide the trip.

Considering a great variety of simulated cases, both proposed and conventional methods presented security for all external events. However, the proposed method presented the best performance and was the fastest for detecting internal faults, even in simultaneous events.

The use of both Clarke and wavelet transforms ensured a great computational efficiency and algorithm simplicity. Indeed, all equations present only addition and multiplication operations, which allows the method to be implemented in hardware environment with a computational burden compatible with the used sampling frequency. In addition, the method was implemented in a real-time simulator, being a quite promising solution for the power transformer protection.

REFERENCES

- [1] J. L. Blackburn and T. J. Domin, *Protective Relaying: Principles and Applications, 3rd Ed.*. Taylor & Francis, 2006.
- [2] W. Elmore, *Protective Relaying: Theory and Applications*, Taylor & Francis, 2003.
- [3] A. K. Pradhan, A. Routray, S. Pati, and D. K. Pradhan, "Wavelet fuzzy combined approach for fault classification of a series-compensated transmission line," *IEEE Trans. Power Del.*, vol. 19, no. 4, pp. 1612–1618, Oct. 2004.

- [4] K. Behrendt, N. Fischer, and C. Labuschagne, "Considerations for using harmonic blocking and harmonic restraint techniques on transformer differential relays," *J. Reliable Power*, vol. 2, no. 3, pp. 36–52, 2011.
- [5] A. Guzman, N. Fischer, and C. Labuschagne, "Improvements in transformer protection and control," in *Proc. 62nd Annu. Conf. Protective Relay Eng.*, Mar. 2009, pp. 563–579.
- [6] S. Hodder, B. Kasztenny, N. Fischer, and Y. Xia, "Low second-harmonic content in transformer inrush currents - analysis and practical solutions for protection security," in *Proc. 67th Annu. Conf. Protective Relay Eng.*, Mar. 2014, pp. 705–722.
- [7] K. Silva and L. Peres, "Power transformer protection using an instantaneous-current-value negative sequence differential element," *Int. J. Elect. Power Energy Syst.*, vol. 108, pp. 96–106, 01 2019.
- [8] D. Barbosa, U. Netto, D. Coury, and M. Oleskovicz, "Power transformer differential protection based on clarke's transform and fuzzy systems," *IEEE Trans. Power Del.*, vol. 26, no. 2, pp. 1212–1220, Apr. 2011.
- [9] L. Zhang, Q. Wu, T. Ji, and A. Zhang, "Identification of inrush currents in power transformers based on higher-order statistics," *Electric Power Syst. Res.*, vol. 146, pp. 161–169, 2017.
- [10] S. Bagheri, Z. Moravej, and G. B. Gharehpetian, "Classification and discrimination among winding mechanical defects, internal and external electrical faults, and inrush current of transformer," *IEEE Trans. Ind. Inform.*, vol. 14, no. 2, pp. 484–493, Feb. 2018.
- [11] H. Esponda, E. Vázquez, M. A. Andrade, and B. K. Johnson, "A setting-free differential protection for power transformers based on second central moment," *IEEE Trans. Power Del.*, vol. 34, no. 2, pp. 750–759, Apr. 2019.
- [12] S. A. Saleh, B. Scaplen, and M. A. Rahman, "A new implementation method of wavelet-packet-transform differential protection for power transformers," *IEEE Trans. Ind. Appl.*, vol. 47, no. 2, pp. 1003–1012, Mar.-Apr. 2011.
- [13] R. P. Medeiros, F. B. Costa, and K. M. Silva, "Power transformer differential protection using the boundary discrete wavelet transform," *IEEE Trans. Power Del.*, vol. 31, no. 5, pp. 2083–2095, Oct. 2016.
- [14] R. P. Medeiros and F. B. Costa, "A wavelet-based transformer differential protection with differential current transformer saturation and cross-country fault detection," *IEEE Trans. Power Del.*, vol. 33, no. 2, pp. 789–799, Apr. 2018.
- [15] R. P. Medeiros and F. B. Costa, "A wavelet-based transformer differential protection: Internal fault detection during inrush conditions," *IEEE Trans. Power Del.*, vol. 33, no. 6, pp. 2965–2977, Dec. 2018.
- [16] F. B. Costa, "Fault-induced transient detection based on real-time analysis of the wavelet coefficient energy," *IEEE Trans. Power Del.*, vol. 29, no. 1, pp. 140–153, Feb. 2014.
- [17] G. Ziegler, *Numerical Differential Protection: Principles and Applications*. Hoboken, NJ, USA: Wiley, 2005.
- [18] H. Ferrer and E. Schweitzer, *Modern Solutions for Protection, Control, and Monitoring of Electric Power Systems*. Schweitzer Engineering Laboratories, Incorporated, 2010.
- [19] A. Guzman, S. Zocholl, G. Benmouyal, and H. Altuve, "A current-based solution for transformer differential protection-Part I: Problem statement," *IEEE Trans. Power Del.*, vol. 16, no. 4, pp. 485–491, Oct. 2002.
- [20] Z. Bo, G. Weller, and T. Lomas, "A new technique for transformer protection based on transient detection," *IEEE Trans. Power Del.*, vol. 15, no. 3, pp. 870–875, Jul. 2000.
- [21] S. E. Laboratories, *SEL-487E-3, -4 Transformer Protection Relay*, 2017. [Online]. Available: https://na.eventscloud.com/file_uploads/f67b7364a38323647b9beb96b7c8d416_487E-3-4_400_IM_20190211-20181115.pdf
- [22] K. A. Tavares and K. Melo Silva, "Evaluation of power transformer differential protection using the ATP software," *IEEE Latin America Trans.*, vol. 12, no. 2, pp. 161–168, Mar. 2014.
- [23] A. P. Bernardes, "A complete model of differential protection of transformers for tests in a digital relay," Master's thesis, Portuguese, USP, Brazil, 2006. [Online]. Available: https://www.tese.usp.br/tese/disponiveis/18/18154/tde-16072006-122259/publico/Dissertacao_M Mestre_AlexandrePacienciaBernardes.pdf
- [24] G. T. Silva, C. R. A. Junior, J. C. Oliveira, A. C. Souza, and I. N. Santos, "Computational implementation of the rio madeira HVDC system," in *Brazilian Symposium on Electrical Systems*, May 2018, pp. 1–6.
- [25] B. Kasztenny *et al.*, "Exploring the IEEE C37.234 guide for protective relay application to power system buses," in *Proc. 64th Annu. Conf. Protective Relay Eng.*, 2011, pp. 29–36.

- [26] L. E. Center, *Alternative Transients Program (ATP): Rule Book. EMTP, 1992*. [Online]. Available: <https://books.google.com.br/books?id=VmzynAEACAAJ>
- [27] IEEE Power System Relaying Committee, "Emtp reference models for transmission line relay testing," 2004. [Online]. Available: <https://www.pes-psrc.org/kb/published/reports/EMTP%20Ref%20Model-Final.pdf>
- [28] A. G. Phadke and J. S. Thorp, *Synchronized Phasor Measurements and Their Applications*, New York, NY, USA: Springer, 2008.



Rodrigo Prado Medeiros received the B.Sc., M.Sc., and Ph.D. degrees in electrical engineering from the Federal University of Rio Grande do Norte (UFRN), Natal, Brazil, in 2012, 2014, and 2018, respectively. From 2019 to 2020, he was a Postdoctoral Researcher with UFRN. He is currently a Professor with the Federal Rural University of the Semi-Arid, Caraiúbas, Brazil. His research interests include power system protection, electromagnetic transients, and electric power quality.



Flavio Bezerra Costa (Member, IEEE) received the B.Sc., M.Sc., and Ph.D. degrees in electrical engineering from the Federal University of Campina Grande (UFCG), Campina Grande, Brazil, in 2005, 2006, and 2010, respectively. He is currently a Professor with the Federal University of Rio Grande do Norte, School of Science and Technology, Natal, Brazil.

In 2010, he was a Postdoctoral Researcher with UFCG, from 2011 to 2012, he was a Visiting Researcher with Katholieke Universiteit Leuven, Leuven, Belgium, in 2014, he was a Visiting Researcher

with INESC TEC - Institute for Systems and Computer Engineering, Technology and Science, Porto, Portugal, from 2014 to 2015, he was a Postdoctoral Researcher with RWTH Aachen University, Aachen, Germany, and from 2018 to 2019, he was a Visiting Professor with the Technical University of Berlin, Berlin, Germany. His current research interests include power system protection, electric power quality, control of renewable energy systems, and smart-grid solutions.



Kleber Melo Silva (Senior Member, IEEE) received the B.Sc., M.Sc., and Ph.D. degrees in electrical engineering from the Federal University of Campina Grande, Campina Grande, Brazil, in 2004, 2005, and 2009, respectively. Since 2009, he has been a Professor with the University of Brasília, Brasília, Brazil, and the Head of the Power System Protection Group. From 2019 to 2020, he was a Visiting Professor with the Texas A&M University, College Station, TX, USA. His research interests include power system protection, fault location, and electromagnetic transients.

He is the Editor of the IEEE TRANSACTIONS ON POWER DELIVERY and a Member of SC B5-Protection and Automation Committee of Cigre Brazil.



Jose de Jesus Chavez Muro (Member, IEEE) received the M.Sc. and Ph.D. degrees from the Center for Research and Advanced Studies, National Polytechnic Institute, Mexico City, Mexico, in 2006 and 2009, respectively. In 2009, he was a Visiting Ph.D. with Real-Time Experimental Laboratory, the University of Alberta, Edmonton, Canada. He joined the Technological Institute of Morelia, Morelia, Mexico, as an Assistant Professor in 2010, a Full Professor in 2012, and the Chair of the Graduate and Research Program in electrical engineering from 2014 to 2016.

He was a Postdoctoral Member with the Delft University of Technology, Delft, The Netherlands. He is currently a Professor with the National Technological Institute of Mexico, Mexico City, Mexico. His research interests include electromagnetic transients, harmonics analysis, digital protective relays, wide-area protection, and real-time simulation.



José Raimundo Lima Júnior received the M.Sc. degree in electrical engineering from the Federal University of Campina Grande, Campina Grande, Brazil, in 2013. Since 2005, he has been with São Francisco Hydroelectrical Company (CHESF), Brazil performing power system protection studies and managing transmission enterprises. He is currently an Assistant Professor with the University of Pernambuco, Recife, Brazil. His research interests include power system protection and electromagnetic transients.



Marjan Popov (Senior Member, IEEE) received the Dipl.-Ing. degree in electrical power engineering from Ss. Cyril and Methodius University, Skopje, the Republic of Macedonia and the Ph.D. degree in electrical power engineering from the Delft University of Technology, Delft, The Netherlands, in 1993 and 2002, respectively. He is also a Chevening Alumnus and, in 1997, he was an Academic Visitor with the University of Liverpool, Liverpool, U.K., he is currently with Arc Research Group in modeling SF6 circuit breakers. His main research interests include future power

systems, large-scale power system transients, intelligent protection for future power systems, and wide-area monitoring and protection. He is a Member of Cigré and actively participated in WG C4.502 and WG A2/C4.39. In 2010, he received the prestigious Dutch Hidde Nijland Prize for extraordinary research achievements. He was the recipient of the IEEE PES Prize Paper Award and the IEEE Switchgear Committee Award in 2011. He is an Associate Editor for the *Elsevier's International Journal of Electrical Power and Energy Systems*. In 2017, together with the Dutch utilities TenneT, Alliander and Stedin he founded the Dutch Power System Protection Centre to promote the research and education in power system protection.